HHS Public Access

Author manuscript

Mol Cell Neurosci. Author manuscript; available in PMC 2018 June 21.

Published in final edited form as:

Mol Cell Neurosci. 2018 April ; 88: 342–352. doi:10.1016/j.mcn.2018.03.005.

CaBP1 regulates Ca_v1 L-type Ca^{2+} channels and their coupling to neurite growth and gene transcription in mouse spiral ganglion neurons

Tian Yang[1], **Ji-Eun Choi**[1], **Daniel Soh**[1], **Kevin Tobin**[1], **Mei-ling Joiner**[2], **Marlan Hansen**[2,3], and **Amy Lee**[1,2,4]

[1]Department of Molecular Physiology and Biophysics, University of Iowa, Iowa City, IA 52242, USA

[2]Department of Otolaryngology Head-Neck Surgery, University of Iowa, Iowa City, IA 52242, USA

[3]Department of Neurosurgery, University of Iowa, Iowa City, IA 52242, USA

[4]Department of Neurology, University of Iowa, Iowa City, IA 52242, USA

Introduction

In neurons, voltage-gated Ca_v Ca^{2+} channels convert electrical signals into discrete elevations in intracellular Ca^{2+} that initiate a wide range of signaling cascades. Of the multiple classes of Ca_v channels, Ca_v1 L-type channels are key mediators of Ca^{2+} signals controlling neurogenesis (Marschallinger et al., 2015; Temme et al., 2016; Volkening et al., 2017), neurite growth (Audesirk et al., 1990; Robson and Burgoyne, 1989; Roehm et al., 2008; Schindelholz and Reber, 2000), and gene transcription (Dolmetsch et al., 2001; Graef et al., 1999; Oliveria et al., 2007). Mutations affecting the major Ca_v1 channels in the brain, $Ca_v1.2$ and $Ca_v1.3$, are linked to a variety of neurological and psychiatric disorders (Kabir et al., 2017; Pinggera and Striessnig, 2016). Thus, factors that regulate Ca_v1 channels may be critical for maintaining the balance between normal and diseased states of the nervous system.

A major regulator of Ca_v1 channels is calmodulin (CaM). Constitutively associated with the pore-forming Ca_v α_1 subunit, CaM promotes inactivation of the channel upon binding to Ca^{2+} (Ben-Johny and Yue, 2014). Ca^{2+}-dependent inactivation (CDI) of Ca_v1 channels is crucial for controlling excitability in the heart (Alseikhan et al., 2002), but a variety of factors may oppose CDI of Ca_v1 channels in neurons. In particular, members of a family of

Corresponding author: Amy Lee, Dept. of Molecular Physiology and Biophysics, University of Iowa, PBDB 5318, 169 Newton Road, Iowa City, IA 52242, Phone: (319) 384-1762, Fax: (319) 335-7330, amy-lee@uiowa.edu.

Competing Interests

The authors declare no competing interests.

Author contributions

All experiments were performed at the University of Iowa. TY and AL conceived and designed the work. TY, JC, DS, KT, and MJ contributed the acquisition and/or interpretation of the data. All authors contributed to the drafting of the manuscript or revising it for important intellectual content, approval of the final version of the manuscript, and agree to be accountable for all aspects of the work. All persons designated as authors qualify for authorship, and all those who qualify for authorship are listed.

Ca^{2+} binding proteins (CaBPs) related to CaM are highly expressed in neural tissues (Haeseleer et al., 2000) and suppress CDI in heterologous expression systems (Hardie and Lee, 2016). The mechanism is thought to involve competitive displacement of CaM from the channel complex (Findeisen et al., 2013; Zhou et al., 2004) as well as allosteric modulation (Oz et al., 2013; Yang et al., 2014).

CaBPs are highly expressed in the retina where they may regulate the contribution of Ca_V1 channels to neurotransmitter release at ribbon synapses (Haeseleer et al., 2004; Haeseleer et al., 2000; Rieke et al., 2008; Sinha et al., 2016). CaBPs are also expressed in cochlear hair cells, where it was hypothesized that their antagonism of CaM may account for the very limited CDI of $Ca_V1.3$ channels (Cui et al., 2007; Yang et al., 2006). Of the multiple CaBP family members, CaBP2 is specifically enriched in inner and outer hair cells (Cui et al., 2007; Yang et al., 2016). However, CDI of $Ca_V1.3$ in inner hair cells of CaBP2 knock-out mice was not affected (Picher et al., 2017), despite the fact that CaBP2 strongly suppresses CDI of $Ca_V1.3$ channels in transfected HEK293 cells (Schrauwen et al., 2012). Thus, whether CaBPs regulate CDI of Ca_V1 channels in neuronal cell-types remains to be established.

Expressed at higher levels in the cochlea than CaBP2, CaBP1 is particularly enriched in spiral ganglion neurons (SGNs, (Yang et al., 2016)) which transmit sound information from hair cells to the brain via the auditory nerve. Alternative splicing gives rise to three CaBP1 variants (CaBP1-S, CaBP1-L, and caldendrin), of which caldendrin is the most abundant in the cochlea (Yang et al., 2016). To elucidate the cellular functions of CaBP1, we analyzed the properties of Ca_V1 channels and Ca_V1 signaling pathways in SGNs of mice lacking all three variants (C-KO; (Kim et al., 2014)). Our results indicate that CaBP1 suppresses CDI of Ca_V1 channels in SGNs and is necessary for the contribution of Ca_V1 channels to excitation-transcription coupling and the activity-dependent repression of neurite outgrowth. Our study provides the first evidence that CaBPs modulate CDI of Ca_V1 channels in neurons, and highlights the diverse roles of CaBPs in regulating Ca_V Ca^{2+} signaling in the nervous system.

Materials and Methods

Ethical Approval

All experiments were performed in accordance with guidelines set by the Office of the Institutional Animal Care and Use Committee at the University of Iowa. The procedures used in this study are not expected to produce pain or suffering in the animals. Generation of C-KO mice (RRID: MGI: 5780462) was described previously (Kim et al., 2014). Mice were maintained on a C57BL/6 (Envigo) background and housed in groups on a standard 12:12 hour light: dark cycle, with food and water provided ad libitum. Mice from post-natal days (P) 3–7 of mixed sexes were used in this study.

Electrophysiological recordings of SGNs

Dissociated SGN cultures were prepared according to a previously described protocol (Lv et al., 2012) with modification. Briefly, cochlear tissue was dissected from 2–4 mice in

Ca^{2+}/Mg^{2+}-free Hank's Balanced Salt Solution (HBSS) and digested in an enzyme mixture containing collagenase type I (1 mg/mL, ThermoFisher 17100) and DNase I (1 mg/mL, Sigma DN25) at 37°C for 25 min. After gentle triturations, the cells were plated on poly-L-ornithine/laminin-coated coverslips in Nunclon 4-Well PS MultiDish (Thermo Scientific). SGNs were maintained in Neurobasal-A culture media supplemented with 2% B27 (v/v), 2 mM L-glutamine, 1x penicillin-Streptomycin, 25 ng/mL BDNF (Sigma B3795) and 25 ng/mL NT3 (Sigma N1905). All media and supplements were from Gibco unless noted otherwise.

About 24–72 h after plating SGNs (cultures prepared from P5-P7 mice), whole-cell patch clamp recordings were performed at room temperature. Data were acquired with an EPC-10 patch clamp amplifier and Patchmaster software (HEKA Elektronik) and analyzed with Igor Pro software (Wavemetrics). Electrodes (3–5 MΩ) were pulled from borosilicate glass and were filled with solution containing (in mM): 70 CsCl, 70 N-methyl-D-glucamine chloride, 1 $CaCl_2$, 10 HEPES, 10 EGTA, 4 MgATP, pH 7.2. The external solution contained (in mM): 120 choline-Cl, 20 tetraethylammonium chloride (TEA-Cl), 5 4-aminopyridine (4-AP), 0.02 linopirdine, 2 CsCl, 5 $CaCl_2$ or 5 $BaCl_2$, 0.5 $MgCl_2$, 10 HEPES, 5 D-glucose, pH 7.40. As described previously (Lv et al., 2014; Lv et al., 2012), the following criteria were used for inclusion of data: (1) establishment of stable giga-ohm seal for at least 5 min before data collection; (2) currents did not show signs of voltage-clamp error or contamination by outward currents; (3) absence of current rundown.

Current-voltage relations were analyzed with depolarizing voltage ramps from a holding potential of −45 mV to +70 mV in 320 ms. The current amplitude was divided by the cell capacitance to generate the current density–voltage (I–V) relationship. I–V curves were fit with the following equation: $I = G(V - E)/\{1 + \exp[(V - V_{1/2})/k]\}$ where G is conductance, V is the test potential, E is the reversal potential, $V_{1/2}$ is the voltage for half-maximal activation, and k is the slope factor. Inactivation was analyzed with depolarizing voltage 1-s steps from a holding potential of −45 mV to 0 (for I_{Ca}) or −10 mV (I_{Ba}). Different voltages were used due to account for the negative shift in voltage-dependent activation of I_{Ba} compared to I_{Ca} caused by surface charge screening effects (Wilson et al., 1983). Inactivation was determined by dividing the amplitude of the residual current at the end of the pulse with that of the peak current.

Analysis of SGN survival and neurite growth

Dissociated spiral ganglion cultures were prepared as previously described (Hegarty et al., 1997) (Hansen et al., 2001). For each culture, 4 mice were used. Briefly, the spiral ganglia were dissected from P3-P5 mouse pups in Ca^{2+}/Mg^{2+}-free HBSS, and enzymatically digested with 0.1% collagenase and 0.125% trypsin. After mechanical dissociation, the cells were plated on coverslips coated with poly-L-ornithine/laminin in 8-well culture chambers (Nalge Nunc International). Cells were maintained in N2 media, ingredient as follows: high glucose Dulbecco's Modified Eagle's Medium (DMEM), 1x N2 supplement (Invitrogen; Carlsbad, CA), insulin (10 μg/ml, Sigma-Aldrich), and 1x penicillin/streptomycin. Cells were kept in a humidified incubator at 37 °C with 5% CO_2.

Four hours after plating, SGNs were placed in control (5.4 mM K^+) or depolarizing conditions (various K^+ concentrations) prior to analysis of survival or neurite appearance. To evaluate the contribution of Ca_v1 channels, the solution contained isradipine (0.1 μM or 10 μM, TOCRIS), (±)-Bay K 8644 (0.1 μM or 10 μM, TOCRIS), or DMSO (0.1%). Following incubation, SGNs were fixed in 4% paraformaldehyde (PFA) in phosphate-buffered saline (PBS) for 15 min, and then in blocking buffer (5% normal goat serum and 0.5% Triton-X in PBS) for 1 h at room temperature (RT). SGNs were labeled with primary anti-neurofilament 200 (NF200) monoclonal antibody (1:500, Sigma-Aldrich Cat# N0142 RRID: AB_477257) in blocking buffer for 1 h at RT. After 3 washes in 1X PBS (5 min each), SGNs were incubated with secondary antibodies conjugated with Alexa 568 (1:500, ThermoFisher, Cat# A-11019, RRID: AB_143162) in blocking buffer and DAPI for 1 h at RT. The cells were washed 3 times in 1x PBS before mounting with glycerol and analyzing with an Olympus BX53 microscope equipped with Olympus DP72 camera and CellSens Standard imaging software (RRID: SCR_014551).

Quantitative analysis was performed by researchers blinded to experimental conditions. For analysis of SGN survival, all neurons were counted in each well following exposure to control or experimental conditions. For analysis of neurite growth, images were taken for all SGNs with visible neurites. Neurite length was defined as the maximal possible distance along a neurite and determined for each SGN using the measurement tool in Image J (NIH; RRID: SCR_003070). If there was more than one neurite, the longest branch was quantified. If the longest neurite extended beyond the field of the image, additional images were acquired and automatically stitched together using CellSens software. All the data were compiled with Excel. To obtain the percentage of neurons with neurites, the number of SGNs with neurites longer than 10 μm was normalized to the total number of SGNs in each well.

Phosphorylated CREB assays

Measurement of CREB phosphorylation following depolarization was performed as described previously (Hansen et al., 2003). Briefly, SGN cultures were prepared as described for survival/neurite growth assays and were incubated with 0.1% DMSO (control) or 10 μM isradipine for 30 min at 37 °C, and stimulated with the same medium containing 5.4 mM K^+ or 30 mM K^+ for 15 min at RT. Neurons were immediately fixed with 4% PFA and proceed with immunocytochemistry described above except that cells were also incubated in anti-phospho-CREB (Ser133) monoclonal antibody (1:350, Cell Signaling Technology Cat# 9198, RRID: AB_2561044) and Alexa 647 (1:500, Thermo Fisher Scientific Cat# A21246, RRID: AB_10375565). Images of SGNs were taken with Olympus Fluoview 1000 confocal laser scanning microscope with a 60x lens and FluoView software (RRID: SCR_014215), and analyzed with ImageJ software. The region of interest was outlined from DAPI staining, and pCREB intensity was measured as mean grey value in arbitrary units of pixel intensity. The imaging and quantification were performed by researchers blinded to genotype and conditions.

Ca^{2+} imaging

SGN cultures were prepared as for electrophysiology experiments except that the cells were maintained in N2 media supplemented with BDNF (25 ng/mL) and NT3 (25 ng/mL). About 12–16 hours after plating, SGNs were infected by adenoassociated virus (AAV1) expressing GCaMP3 under a synapsin promoter (AAV1.CMV.PI.SynGCaMP3.SV40, Vectorcore, University of Pennsylvania). Ca^{2+} imaging was performed 24–48 hours after the infection. SGNs were kept in 5 mM K^+ control solution (in mM: 119 NaCl, 23 $NaHCO_3$, 10 glucose, 1.25 NaH_2PO_4, 5 KCl, 2 Na-Pyruvate, 3 $CaCl_2$, and 1 $MgCl_2$) and then stimulated with 80 mM K^+ solution (same as control solution except with 44 mM NaCl and 80 mM KCl). Bath solutions were continuously perfused by gravity. Images were taken at 1 frame per second with Olympus Fluoview 1000 confocal laser scanning microscope with a 40x water immersion lens and FluoView software and analyzed with ImageJ software. TurboReg (RRID: SCR_014308) was used to align images when there was shift during imaging.

The evoked Ca^{2+} signal (F/F_0) was measured by normalizing the maximal fluorescence intensity (F = average of the maximum signal detected in 3 frames after the 80 mM K^+ stimulation) to the baseline fluorescence (F_0 = average of the signal in the first 3 frames recorded after time zero). For some experiments, isradipine (10 μM) was applied to the cells between two applications of 80 mM K^+ solution. In these experiments, the evoked Ca^{2+} signal (F/F_b) was measured by normalizing the maximal fluorescence intensity (F = average of the maximal signal detected in 3 frames after applying isradipine) to the baseline fluorescence (F_b = average of the minimum signal in 3 frames after applying isradipine but before the second application of 80 mM K^+).

Experimental design and statistical analysis

For all experiments, male and female mice were used. Whenever possible, WT and C-KO samples were prepared and analyzed in parallel. Statistical analysis was done with Graphpad Prism software 7 (RRID: SCR_002798) unless noted otherwise. An alpha level of 0.05 was used for all statistical tests. Data were first tested for normality by Shapiro-Wilk normality test. If the data were normally distributed, unpaired *t* test or ANOVA with post hoc Bonferroni's multiple comparisons test was performed. Otherwise, Mann-Whitney test, or Kruskal-Wallis test were performed. For 2-way ANOVA test, the main effects were reported if there was no significant interaction, and post hoc analysis was performed on the main effects that had more than two levels. Otherwise, post hoc tests were performed and simple main effects were reported using adjusted *p* value for multiple comparisons. To analyze the change in distribution of neurite lengths between 12 h to 24 h, neurite lengths were binned to 100 μm bin-width (except neurites longer than 410 μm were binned as 1 group), and Chi-square test was performed. Three significant digits for *p* values were reported. Error bars represented standard deviation (SD) unless otherwise noted.

Results

CDI of Ca_V channels is enhanced in C-KO SGNs

Based on the effects of CaBP1 on Ca_V1 channel CDI in heterologous expression systems (reviewed in (Hardie and Lee, 2016)), we hypothesized that CaBP1 should support Ca_V1-

mediated Ca^{2+} signaling in SGNs by suppressing CDI. If so, CDI should be greater in SGNs lacking CaBP1 expression. To test this prediction, we characterized the properties of Ca^{2+} currents (I_{Ca}) and Ba^{2+} currents (I_{Ba}) in whole-cell patch clamp recordings of SGNs in culture from wild-type (WT) and C-KO mice. Although low-voltage activated Ca_v3 channels are expressed in SGNs, we minimized their contribution by maintaining the holding potential at −45 mV (Lv et al., 2012). In current-voltage (I–V) analyses using ramp protocols, there was no significant difference in peak current densities or parameters for voltage-dependent activation in WT and C-KO SGNs (Fig. 1A,B; Table 1). Thus, genetic silencing of CaBP1 did not affect the activation properties of Ca_v currents in SGNs.

Inactivation was measured as the current amplitude at the end of a depolarizing pulse normalized to the peak current amplitude (I_{res}/I_{pk}) for I_{Ca} and I_{Ba}. Since Ba^{2+} binds to CaM poorly (Wang, 1985), I_{Ba} exhibits voltage dependent inactivation that is much slower than the rapid inactivation of I_{Ca} due to CDI. Although Ca_v2 channels are expressed in SGNs (Chen et al., 2011; Lv et al., 2012), we isolated CDI mediated by Ca_v1 channels by exploiting the reliance of CDI of Ca_v2 channels on global Ca^{2+} elevations that are readily blocked by Ca^{2+} chelators (e.g., EGTA, BAPTA). Since Ca_v1 channel CDI depends on local Ca^{2+} signals within a nanodomain of the channel pore (reviewed in (Christel and Lee, 2012)), greater inactivation (*i.e.,* smaller I_{res}/I_{pk}) of I_{Ca} compared to I_{Ba} in the presence of EGTA (10 mM in the intracellular recording solution) should reflect CDI of Ca_v1 channels (Huang et al., 2012). CDI was evident in both WT and C-KO SGNs in that I_{res}/I_{pk} was indeed smaller for I_{Ca} than for I_{Ba} (Fig. 1C,D). Using the difference in I_{res}/I_{pk} for I_{Ca} and I_{Ba} as a metric for CDI (F_{CDI}; (Thomas and Lee, 2016)) we noted significantly greater CDI in C-KO than in WT neurons (~1.7-fold; Fig. 1E). These results support a role for CaBP1 in suppressing CDI of Ca_v1 currents in SGNs.

Activity-dependent enhancement of SGN survival is not affected in C-KO cultures

Ca^{2+} influx through Ca_v1 channels mediates the prosurvival effects of depolarization in many neurons (Collins et al., 1991) including rat SGNs (Hegarty et al., 1997; Roehm et al., 2008; Shen et al., 2016). To determine if activity-dependent increases in SGN survival differed in WT and C-KO cultures, we used a survival assay modified from previous studies of rat SGNs (Hegarty et al., 1997; Roehm et al., 2008). Neurotrophin-3, which augments SGN survival and neurite growth in culture (Hegarty et al., 1997), was omitted from the culture medium in order to maximize any difference between genotypes. SGN survival was assessed as the percentage of neurons remaining after a prolonged exposure (44 hours) to varying concentrations of extracellular K^+ ($[K^+]_o$). While this approach may seem non-physiological, it should be noted that dissociated SGNs in culture (mostly type I SGNs) are electrically silent as they do not receive innervation from inner hair cells. To mimic electrical activity under these conditions, elevated concentrations of $[K^+]_o$ are used. This is a widely-used strategy for dissecting the contributions of Ca_v1 channels to transcriptional regulation (Wheeler et al., 2012) and activity-dependent repression of neurite growth (Enes et al., 2010). In agreement with previous work (Hegarty et al., 1997), there was a biphasic effect of $[K^+]_o$ on SGN survival with maximal survival at 30 mM for both WT and C-KO cultures. However, there was no difference in the survival of SGNs from WT and C-KO mice under

these conditions (Fig. 2). Thus, CaBP1 is dispensable for the effects of depolarization on the survival of SGNs in culture.

Activity-dependent repression of neurite growth is relieved in C-KO SGNs

To determine if other Ca_v1-regulated signaling pathways were affected in C-KO SGNs, we analyzed activity-dependent repression of neurite regrowth. During dissociation, SGN axons are sheared off but regenerate and grow to lengths >600 μm with time in culture (Hegarty et al., 1997). Neurite regrowth in vitro is inhibited by depolarization-mediated Ca^{2+} influx (Roehm et al., 2008). We hypothesized that the Ca^{2+}-dependent brake on neurite regrowth should be lessened in C-KO SGNs, possibly due to greater CDI of Ca_v1 channels (Fig. 1C–E). To test this, we compared the number of WT and C-KO SGNs with neurites following exposure to varying concentrations of $[K^+]_o$. In contrast to previous findings (Roehm et al., 2008), increasing $[K^+]_o$ did not significantly affect the number of WT SGNs with neurites (Fig. 3A; $H(5) = 7.043$, $p = 0.218$ by Kruskal Wallis test), perhaps due the absence of neurotrophin-3 in our cultures. However with increasing $[K^+]_o$, the number of C-KO SGNs with neurites was significantly greater ($H(5) = 22.19$, $p < 0.001$, by Kruskal-Wallis test), particularly with $[K^+]_o \geq 30$ mM (Fig. 3B).

If CaBP1 represses the initiation rather than the growth of neurites, then there should be a larger time-dependent increase in the number but not the length of neurites in C-KO than SGN cultures. To test this prediction, we compared the increase in the number of SGNs with neurites between 12 and 24 hours of depolarization. In this and subsequent experiments, 30 mM $[K^+]_o$ was used for depolarization since neuronal survival was maximal at this concentration (Fig. 2). This concentration of $[K^+]_o$ should produce ~30 mV change in the membrane potential, which falls within the range of depolarization required for SGNs to reach firing thresholds (Liu et al., 2014). Between 12 and 24 hours of depolarization, the increase in SGNs with neurites was significantly greater in C-KO than WT cultures (Fig. 4A–C). However, neurite lengths did not undergo as large of an increase in C-KO as in WT cultures ($\chi^2(4) = 16.82$, $p = 0.002$, by Chi-square test; Fig. 4D,E). Therefore, loss of CaBP1 enhances the activity-dependent initiation but not rate of growth of SGN neurites.

Ca_v1 regulation of neurite growth is disrupted in C-KO SGNs

To determine if the contribution of Ca_v1 channels to the regulation of neurite growth is altered in C-KO SGNs, we used the Ca_v1 antagonist isradipine. In WT cultures, isradipine (0.1 μM) caused ~10% increase in the proportion of SGNs with neurites (Fig. 5A). This was not due to greater survival of WT SGNs, which was not affected by isradipine at this concentration (Table 2). A higher concentration (10 μM) of isradipine strongly inhibited survival of WT SGNs (Table 2), which may explain why neurite growth of WT SGNs was not further potentiated at this dose (Fig. 5A). In contrast to its effects on WT SGNs, isradipine did not alter the percent of C-KO SGNs with neurites following depolarization (Fig. 5B).

We next tested if the Ca_v1 agonist Bay K 8644 would, like isradipine, have a weaker effect on neurite growth of SGNs in C-KO than in WT cultures. Consistent with a role for Ca_v1 channels in suppressing neurite growth, Bay K 8644 caused a dose-dependent decline in the

number of WT SGNs with neurites following depolarization (Fig. 6A). However, this effect could have resulted from toxicity since WT SGN survival was significantly reduced in the presence of Bay K 8644. In contrast to its effects on WT SGNs, Bay K 8644 had no significant effect on either neurite growth or survival of C-KO SGNs. Taken together, these results indicate an uncoupling of Ca_v1 Ca^{2+} signals from activity-dependent regulation of neurite growth and survival in C-KO SGNs.

Ca_v1 coupling to transcriptional regulation is impaired in C-KO SGNs

A prominent Ca_v1 signaling pathway in many neurons involves the activity-dependent phosphorylation of cAMP response element binding protein (CREB) – a transcription factor that regulates synaptic plasticity underlying learning and memory (Bengtson and Bading, 2012). In neurons, Ca_v1 channels are tightly coupled to increases in phosphorylated CREB (pCREB) levels which can be measured by immunofluorescence (Wheeler et al., 2012). Based on the reduced contribution of Ca_v1 channels to the regulation of neurite growth in C-KO SGNs, we hypothesized that Ca_v1 signaling to pCREB would be diminished in C-KO SGNs. To test this, we measured pCREB levels by immunofluorescence in WT and C-KO SGNs following exposure to a basal (5 mM) and depolarizing (30 mM) concentration of KCl. Although depolarization caused a robust increase in pCREB in both WT and C-KO SGNs, this increase was significantly blunted in C-KO compared to WT SGNs (Fig. 7A–C). Consistent with the lack of effect of isradipine in C-KO SGNs in neurite growth assays (Fig. 5B), pCREB induction by depolarization was prevented by isradipine (10 μM) in WT but not C-KO SGNs (Fig. 7A–C). Thus, the contribution of Ca_v1 channels to pCREB activation is also severely impaired in C-KO SGNs.

We also compared the magnitude of Ca_v1-mediated Ca^{2+} signals in WT and C-KO SGNs transfected with the genetically encoded Ca^{2+} indicator GCaMP3. Depolarization with 80 mM $[K^+]_o$ caused a marked increase in GCaMP3 fluorescence in WT SGNs which was significantly weaker in C-KO SGNs (Fig. 8A,B). Consistent with evidence for other Ca_v channels besides Ca_v1 in SGNs (Lv et al., 2014; Lv et al., 2012), the evoked GCaMP3 signal was reduced but not abolished by isradipine in WT SGNs (Fig. 8A,C). The isradipine-insensitive Ca^{2+} signal was not significantly different in C-KO and WT SGNs (Fig. 8A,C), which suggested that the contribution of Ca_v channels other than Ca_v1 is not affected by CaBP1 knockdown and that the major reduction in the depolarization-evoked Ca^{2+} signal in C-KO compared to WT SGNs is due to loss of function of Ca_v1 channels.

Discussion

CaBP1 regulates CDI of Ca_v1 channels in SGNs

Despite a wealth of evidence that CaBP1 modulates $Ca_v1.2$ and $Ca_v1.3$ channels in heterologous expression systems (reviewed in (Hardie and Lee, 2016)), our study is the first to demonstrate that CaBP1 regulates CDI of Ca_v1 channels in neurons. The increase in CDI in C-KO SGNs is relatively modest considering that coexpression of CaBP1 with $Ca_v1.2$ and $Ca_v1.3$ nearly abolishes CDI in transfected HEK293 cells (Cui et al., 2007; Zhou et al., 2004). This discrepancy could stem from caldendrin being the major CaBP1 splice variant expressed in SGNs (Yang et al., 2016). In transfected cells, caldendrin has a more moderate

effect than the other CaBP1 variants in suppressing CDI (Tippens and Lee, 2007). It is also possible that CDI is suppressed in SGNs by factors in addition to CaBP1. For example, alternative splicing and RNA editing can produce Ca_V1 channels in neurons with limited CDI (Bazzazi et al., 2013; Shen et al., 2006; Singh et al., 2008; Tan et al., 2011). It is noteworthy that knock-out of CaBP2 causes increased voltage-dependent inactivation rather than CDI of the $Ca_V1.3$ current in inner hair cells (Picher et al., 2017), despite evidence that CaBP2 strongly suppresses CDI of $Ca_V1.3$ channels in transfected HEK293T cells (Schrauwen et al., 2012). Clearly, the native environment in which Ca_V channels are expressed may strongly influence the extent to which Ca_V channels are modulated by CaBPs.

CaBP1 enables activity-dependent coupling of Ca_V1 channels to pCREB

Intuitively, stronger CDI in C-KO SGNs might lead to weaker, more transient Ca_V1-mediated Ca^{2+} signals that would be insufficient to support activity-dependent CREB phosphorylation. However, it is also possible that CaBP1 may couple Ca_V1 channels to pCREB independent of its effects on CDI. In analyses of cortical neurons in culture, mutation of a CaM binding site (IQ-domain) in the proximal C-terminal domain of $Ca_V1.2$ reduces activity-dependent phosphorylation of CREB independent of any changes in Ca_V1-mediated Ca^{2+} signals (Dolmetsch et al., 2001). Mutations in the $Ca_V1.2$ IQ domain also disrupt CaBP1 binding (Zhou et al., 2005), and CaBP1 is highly expressed in cortical neurons (Kim et al., 2014). Thus, CaBP1 rather than CaM binding to the IQ-domain may be required for excitation-transcription coupling in neurons. Understanding precisely how CaBP1 enables Ca_V1 signaling to the nucleus in SGNs, and perhaps more broadly in other neurons, is an important challenge for future studies.

CaBP1 is necessary for activity-dependent repression of SGN neurite growth

While it promotes axon growth of retinal ganglion neurons (Goldberg et al., 2002) and sympathetic motor neurons (Singh and Miller, 2005), electrical activity suppresses axon growth of dorsal root ganglion neurons (Fields et al., 1990; Robson and Burgoyne, 1989). Depolarization of dissociated dorsal root ganglion cells with high $[K^+]_o$ or electrical stimulation inhibits the regeneration of their axons, which is blunted by genetic or pharmacological inactivation of $Ca_V1.2$ channels as well as blockers of transcription (Enes et al., 2010). Similarly, depolarization acts as a brake on neurite growth of SGNs, although Ca_V2 as well as Ca_V1 channels are involved (Roehm et al., 2008). Our findings that neurite growth is less repressed by depolarization in C-KO than WT SGNs (Fig. 3B) could be explained by weaker Ca_V1 Ca^{2+} signals due to increased CDI, and limited pCREB-dependent transcription (Fig. 9). Ca_V1 coupling to other signaling molecules would also be impaired such as the Ca^{2+}-dependent protease, calpain. For example, Ca_V1-mediated Ca^{2+} influx strongly activates calpain in many cell-types (Jacquemet et al., 2016), and calpain inhibitors relieve activity-dependent block of SGN neurite growth (Roehm et al., 2008). In addition, CaBP1 interacts with a variety of other regulators of Ca^{2+} signaling including inositol trisphosphate receptors (Haynes et al., 2004) and calmodulin-dependent protein kinase II (Haeseleer et al., 2000). Therefore, CaBP1 may regulate SGN neurite growth via multiple mechanisms.

Concluding remarks

During development, the growth potential of axons diminishes upon their forming connections with appropriate targets. In primary sensory neurons, such as in the dorsal root ganglion (DRG), lesioning of the peripheral axon reactivates the genetic program controlling axon regrowth (Yiera and Bradke, 2006). While electrical activity promotes axon growth in some neurons, it halts axon growth in DRGs (Fields et al., 1990) in a manner that depends on Ca_v1 channels (Robson and Burgoyne, 1989). Like DRGs, SGNs extend axons that extend peripherally and centrally. The role of CaBP1 in supporting the function of Ca_v1 channels and their contribution to activity-dependent repression of neurite growth in SGNs may be important during maturation of the auditory system in ensuring that peripheral and central axons remain firmly connected to hair cells in the cochlea and neurons in the cochlear nucleus, respectively.

However, activity-dependent repression of SGN neurite growth presents a challenge for strategies to restore auditory perception with cochlear implants. When inserted into the cochlea of deaf patients, multi-channel cochlear implants mimic synaptic activation of SGNs by lost hair cells but there is a limited ability of up to 8–10 independent electrode channels to accurately transmit sound information that is normally communicated by ~3500 inner hair cells to ~30,000 SGNs. The regrowth of SGN axons towards particular cochlear implant electrodes might improve the tonotopic specificity of SGN activation and improve temporal coding necessary for speech recognition (Rubenstein, 2004). The electrical stimulation provided by cochlear implants is expected to support the survival of SGNs (Hegarty et al., 1997; Miller et al., 2003), but also limit SGN neurite growth (Roehm et al., 2008). In addition to neurotrophin therapy (Budenz et al., 2012), antagonizing CaBP1 signaling could offer a promising approach to overcoming current obstacles in cochlear implant therapies.

Acknowledgments

Funding

This work was supported by grants from the National Institutes of Health (NS084190, DC009433 to A.L.; DC010362 (Iowa Center for Molecular Auditory Neuroscience); Department of Defense (MR130438 to M. H and A.L); and a Carver Research Program of Excellence Award to A.L.

References

Alseikhan BA, DeMaria CD, Colecraft HM, Yue DT. Engineered calmodulins reveal the unexpected eminence of Ca^{2+} channel inactivation in controlling heart excitation. Proc. Natl. Acad. Sci. U. S. A. 2002; 99:17185–17190. [PubMed: 12486220]

Audesirk G, Audesirk T, Ferguson C, Lomme M, Shugarts D, Rosack J, Caracciolo P, Gisi T, Nichols P. L-type calcium channels may regulate neurite initiation in cultured chick embryo brain neurons and N1E-115 neuroblastoma cells. Brain Res Dev Brain Res. 1990; 55:109–120. [PubMed: 1698574]

Bazzazi H, Ben Johny M, Adams PJ, Soong TW, Yue DT. Continuously tunable Ca^{2+} regulation of RNA-edited $Ca_V1.3$ channels. Cell rep. 2013; 5:367–377. [PubMed: 24120865]

Ben-Johny M, Yue DT. Calmodulin regulation (calmodulation) of voltage-gated calcium channels. J. Gen. Physiol. 2014; 143:679–692. [PubMed: 24863929]

Bengtson CP, Bading H. Nuclear calcium signaling. Adv Exp Med Biol. 2012; 970:377–405. [PubMed: 22351065]

Budenz CL, Pfingst BE, Raphael Y. The use of neurotrophin therapy in the inner ear to augment cochlear implantation outcomes. Anat Rec (Hoboken). 2012; 295:1896–1908. [PubMed: 23044834]

Chen WC, Xue HZ, Hsu YL, Liu Q, Patel S, Davis RL. Complex distribution patterns of voltage-gated calcium channel alpha-subunits in the spiral ganglion. Hear Res. 2011; 278:52–68. [PubMed: 21281707]

Christel C, Lee A. Ca^{2+}-dependent modulation of voltage-gated Ca^{2+} channels. Biochim Biophys Acta. 2012; 1820:1243–1252. [PubMed: 22223119]

Collins F, Schmidt MF, Guthrie PB, Kater SB. Sustained increase in intracellular calcium promotes neuronal survival. J. Neurosci. 1991; 11:2582–2587. [PubMed: 1714495]

Cui G, Meyer AC, Calin-Jageman I, Neef J, Haeseleer F, Moser T, Lee A. Ca^{2+}-binding proteins tune Ca^{2+}-feedback to $Ca_V1.3$ channels in auditory hair cells. J. Physiol. 2007; 585:791–803. [PubMed: 17947313]

Dolmetsch RE, Pajvani U, Fife K, Spotts JM, Greenberg ME. Signaling to the nucleus by an L-type calcium channel-calmodulin complex through the MAP kinase pathway. Science. 2001; 294:333–339. [PubMed: 11598293]

Enes J, Langwieser N, Ruschel J, Carballosa-Gonzalez MM, Klug A, Traut MH, Ylera B, Tahirovic S, Hofmann F, Stein V, Moosmang S, Hentall ID, Bradke F. Electrical activity suppresses axon growth through Ca(v)1.2 channels in adult primary sensory neurons. Curr Biol. 2010; 20:1154–1164. [PubMed: 20579880]

Fields RD, Neale EA, Nelson PG. Effects of patterned electrical activity on neurite outgrowth from mouse sensory neurons. J. Neurosci. 1990; 10:2950–2964. [PubMed: 2398369]

Findeisen F, Rumpf CH, Minor DL Jr. Apo states of calmodulin and CaBP1 control CaV1 voltage-gated calcium channel function through direct competition for the IQ domain. J Mol Biol. 2013; 425:3217–3234. [PubMed: 23811053]

Goldberg JL, Espinosa JS, Xu Y, Davidson N, Kovacs GT, Barres BA. Retinal ganglion cells do not extend axons by default: promotion by neurotrophic signaling and electrical activity. Neuron. 2002; 33:689–702. [PubMed: 11879647]

Graef IA, Mermelstein PG, Stankunas K, Neilson JR, Deisseroth K, Tsien RW, Crabtree GR. L-type calcium channels and GSK-3 regulate the activity of NF-ATc4 in hippocampal neurons. Nature. 1999; 401:703–708. 401. [PubMed: 10537109]

Haeseleer F, Imanishi Y, Maeda T, Possin DE, Maeda A, Lee A, Rieke F, Palczewski K. Essential role of Ca^{2+}-binding protein 4, a $Ca_V1.4$ channel regulator, in photoreceptor synaptic function. Nat Neurosci. 2004; 7:1079–1087. [PubMed: 15452577]

Haeseleer F, Sokal I, Verlinde CL, Erdjument-Bromage H, Tempst P, Pronin AN, Benovic JL, Fariss RN, Palczewski K. Five members of a novel Ca^{2+}-binding protein (CABP) subfamily with similarity to calmodulin. J. Biol. Chem. 2000; 275:1247–1260. [PubMed: 10625670]

Hansen MR, Bok J, Devaiah AK, Zha XM, Green SH. Ca2+/calmodulin-dependent protein kinases II and IV both promote survival but differ in their effects on axon growth in spiral ganglion neurons. J Neurosci Res. 2003; 72:169–184. [PubMed: 12671991]

Hansen MR, Zha XM, Bok J, Green SH. Multiple distinct signal pathways, including an autocrine neurotrophic mechanism, contribute to the survival-promoting effect of depolarization on spiral ganglion neurons in vitro. J. Neurosci. 2001; 21:2256–2267. [PubMed: 11264301]

Hardie J, Lee A. Decalmodulation of Cav1 channels by CaBPs. Channels. 2016; 10:33–37. [PubMed: 26155893]

Haynes LP, Tepikin AV, Burgoyne RD. Calcium-binding protein 1 is an inhibitor of agonist-evoked, inositol 1,4,5-trisphosphate-mediated calcium signaling. J. Biol. Chem. 2004; 279:547–555. [PubMed: 14570872]

Hegarty JL, Kay AR, Green SH. Trophic support of cultured spiral ganglion neurons by depolarization exceeds and is additive with that by neurotrophins or cAMP and requires elevation of [Ca2+]i within a set range. J. Neurosci. 1997; 17:1959–1970. [PubMed: 9045725]

Huang H, Tan BZ, Shen Y, Tao J, Jiang F, Sung YY, Ng CK, Raida M, Kohr G, Higuchi M, Fatemi-Shariatpanahi H, Harden B, Yue DT, Soong TW. RNA editing of the IQ domain in $Ca_V1.3$ channels modulates their Ca^{2+}-dependent inactivation. Neuron. 2012; 73:304–316. [PubMed: 22284185]

Jacquemet G, Baghirov H, Georgiadou M, Sihto H, Peuhu E, Cettour-Janet P, He T, Perala M, Kronqvist P, Joensuu H, Ivaska J. L-type calcium channels regulate filopodia stability and cancer cell invasion downstream of integrin signalling. Nat Commun. 2016; 7:13297. [PubMed: 27910855]

Kabir ZD, Martinez-Rivera A, Rajadhyaksha AM. From Gene to Behavior: L-Type Calcium Channel Mechanisms Underlying Neuropsychiatric Symptoms. Neurotherapeutics. 2017; 14:588–613. [PubMed: 28497380]

Kim KY, Scholl ES, Liu X, Shepherd A, Haeseleer F, Lee A. Localization and expression of CaBP1/caldendrin in the mouse brain. Neuroscience. 2014; 268:33–47. [PubMed: 24631676]

Liu Q, Lee E, Davis RL. Heterogeneous intrinsic excitability of murine spiral ganglion neurons is determined by Kv1 and HCN channels. Neuroscience. 2014; 257:96–110. [PubMed: 24200924]

Lv P, Kim HJ, Lee JH, Sihn CR, Fathabad Gharaie S, Mousavi-Nik A, Wang W, Wang HG, Gratton MA, Doyle KJ, Zhang XD, Chiamvimonvat N, Yamoah EN. Genetic, cellular, and functional evidence for Ca2+ inflow through Cav1.2 and Cav1.3 channels in murine spiral ganglion neurons. J. Neurosci. 2014; 34:7383–7393. [PubMed: 24849370]

Lv P, Sihn CR, Wang W, Shen H, Kim HJ, Rocha-Sanchez SM, Yamoah EN. Posthearing Ca^{2+} currents and their roles in shaping the different modes of firing of spiral ganglion neurons. J. Neurosci. 2012; 32:16314–16330. [PubMed: 23152615]

Marschallinger J, Sah A, Schmuckermair C, Unger M, Rotheneichner P, Kharitonova M, Waclawiczek A, Gerner P, Jaksch-Bogensperger H, Berger S, Striessnig J, Singewald N, Couillard-Despres S, Aigner L. The L-type calcium channel Cav1.3 is required for proper hippocampal neurogenesis and cognitive functions. Cell calcium. 2015; 58:606–616. [PubMed: 26459417]

Miller AL, Prieskorn DM, Altschuler RA, Miller JM. Mechanism of electrical stimulation-induced neuroprotection: effects of verapamil on protection of primary auditory afferents. Brain Res. 2003; 966:218–230. [PubMed: 12618345]

Oliveria SF, Dell'Acqua ML, Sather WA. AKAP79/150 anchoring of calcineurin controls neuronal L-type Ca^{2+} channel activity and nuclear signaling. Neuron. 2007; 55:261–275. [PubMed: 17640527]

Oz S, Benmocha A, Sasson Y, Sachyani D, Almagor L, Lee A, Hirsch JA, Dascal N. Competitive and non-competitive regulation of calcium-dependent inactivation in CaV1.2 L-type Ca^{2+} channels by calmodulin and Ca^{2+}-binding protein 1. J. Biol. Chem. 2013; 288:12680–12691. [PubMed: 23530039]

Picher MM, Gehrt A, Meese S, Ivanovic A, Predoehl F, Jung S, Schrauwen I, Dragonetti AG, Colombo R, Van Camp G, Strenzke N, Moser T. Ca2+-binding protein 2 inhibits Ca2+-channel inactivation in mouse inner hair cells. Proc. Natl. Acad. Sci. U. S. A. 2017; 114:E1717–E1726. [PubMed: 28183797]

Pinggera A, Striessnig J. Cav 1.3 (CACNA1D) L-type Ca2+ channel dysfunction in CNS disorders. J. Physiol. 2016; 594:5839–5849. [PubMed: 26842699]

Rieke F, Lee A, Haeseleer F. Characterization of Ca2+-binding protein 5 knockout mouse retina. Invest Ophthalmol Vis Sci. 2008; 49:5126–5135. [PubMed: 18586882]

Robson SJ, Burgoyne RD. L-type calcium channels in the regulation of neurite outgrowth from rat dorsal root ganglion neurons in culture. Neurosci. Lett. 1989; 104:110–114. [PubMed: 2554216]

Roehm PC, Xu N, Woodson EA, Green SH, Hansen MR. Membrane depolarization inhibits spiral ganglion neurite growth via activation of multiple types of voltage sensitive calcium channels and calpain. Mol Cell Neurosci. 2008; 37:376–387. [PubMed: 18055215]

Rubenstein JT. How cochlear implants encode speech. Curr Opin Otolaryngol Head Neck Surg. 2004; 12:444–448. [PubMed: 15377959]

Schindelholz B, Reber BF. L-type Ca2+ channels and purinergic P2X2 cation channels participate in calcium-tyrosine kinase-mediated PC12 growth cone arrest. Eur J Neurosci. 2000; 12:194–204. [PubMed: 10651874]

Schrauwen I, Helfmann S, Inagaki A, Predoehl F, Tabatabaiefar MA, Picher MM, Sommen M, Seco CZ, Oostrik J, Kremer H, Dheedene A, Claes C, Fransen E, Chaleshtori MH, Coucke P, Lee A, Moser T, Van Camp G. A mutation in CABP2, expressed in cochlear hair cells, causes autosomal-recessive hearing impairment. Am J Hum Genet. 2012; 91:636–645. [PubMed: 22981119]

Shen N, Liang Q, Liu Y, Lai B, Li W, Wang Z, Li S. Charge-balanced biphasic electrical stimulation inhibits neurite extension of spiral ganglion neurons. Neurosci. Lett. 2016; 624:92–99. [PubMed: 27163199]

Shen Y, Yu D, Hiel H, Liao P, Yue DT, Fuchs PA, Soong TW. Alternative splicing of the $Ca_V1.3$ channel IQ domain, a molecular switch for Ca^{2+}-dependent inactivation within auditory hair cells. J. Neurosci. 2006; 26:10690–10699. [PubMed: 17050708]

Singh A, Gebhart M, Fritsch R, Sinnegger-Brauns MJ, Poggiani C, Hoda JC, Engel J, Romanin C, Striessnig J, Koschak A. Modulation of voltage- and Ca2+-dependent gating of CaV1.3 L-type calcium channels by alternative splicing of a C-terminal regulatory domain. J. Biol. Chem. 2008; 283:20733–20744. [PubMed: 18482979]

Singh KK, Miller FD. Activity regulates positive and negative neurotrophin-derived signals to determine axon competition. Neuron. 2005; 45:837–845. [PubMed: 15797546]

Sinha R, Lee A, Rieke F, Haeseleer F. Lack of CaBP1/Caldendrin or CaBP2 Leads to Altered Ganglion Cell Responses. eNeuro. 2016; 3

Tan BZ, Jiang F, Tan MY, Yu D, Huang H, Shen Y, Soong TW. Functional characterization of alternative splicing in the C terminus of L-type CaV1.3 channels. J. Biol. Chem. 2011; 286:42725–42735. [PubMed: 21998309]

Temme SJ, Bell RZ, Fisher GL, Murphy GG. Deletion of the Mouse Homolog of CACNA1C Disrupts Discrete Forms of Hippocampal-Dependent Memory and Neurogenesis within the Dentate Gyrus. eNeuro. 2016; 3

Thomas JR, Lee A. Measuring Ca^{2+}-Dependent Modulation of Voltage-Gated Ca^{2+} Channels in HEK-293T Cells. Cold Spring Harb. Protoc. 2016 2016, pdb prot087213.

Tippens AL, Lee A. Caldendrin: a neuron-specific modulator of $Ca_V1.2$ (L-type) Ca^{2+} channels. J. Biol. Chem. 2007; 282:8464–8473. [PubMed: 17224447]

Volkening B, Schonig K, Kronenberg G, Bartsch D, Weber T. Deletion of psychiatric risk gene Cacna1c impairs hippocampal neurogenesis in cell-autonomous fashion. Glia. 2017; 65:817–827. [PubMed: 28230278]

Wang CL. A note on Ca2+ binding to calmodulin. Biochemical and biophysical research communications. 1985; 130:426–430. 130. [PubMed: 4026838]

Wheeler DG, Groth RD, Ma H, Barrett CF, Owen SF, Safa P, Tsien RW. Ca(V)1 and Ca(V)2 channels engage distinct modes of Ca(2+) signaling to control CREB-dependent gene expression. Cell. 2012; 149:1112–1124. [PubMed: 22632974]

Wilson DL, Morimoto K, Tsuda Y, Brown AM. Interaction between calcium ions and surface charge as it relates to calcium currents. J Membr Biol. 1983; 72:117–130. [PubMed: 6304316]

Yang PS, Alseikhan BA, Hiel H, Grant L, Mori MX, Yang W, Fuchs PA, Yue DT. Switching of Ca^{2+}-dependent inactivation of $Ca_V1.3$ channels by calcium binding proteins of auditory hair cells. J. Neurosci. 2006; 26:10677–10689. [PubMed: 17050707]

Yang PS, Johny MB, Yue DT. Allostery in Ca^{2+} channel modulation by calcium-binding proteins. Nat Chem Biol. 2014; 10:231–238. [PubMed: 24441587]

Yang T, Scholl ES, Pan N, Fritzsch B, Haeseleer F, Lee A. Expression and Localization of CaBP Ca2+ Binding Proteins in the Mouse Cochlea. PLoS One. 2016; 11:e0147495. [PubMed: 26809054]

Yiera, B., Bradke, F. Stimulating Intrinsic Growth Potential in Mammalian Neurons. In: Becker, CG., Becker, T., editors. Model Organisms in Spinal Cord Regeneration. Wiley-VCH Verlag GmbH & Co. KGaA; Weinheim, Germany: 2006.

Zhou H, Kim SA, Kirk EA, Tippens AL, Sun H, Haeseleer F, Lee A. Ca^{2+}-binding protein-1 facilitates and forms a postsynaptic complex with $Ca_V1.2$ (L-type) Ca^{2+} channels. J. Neurosci. 2004; 24:4698–4708. [PubMed: 15140941]

Zhou H, Yu K, McCoy KL, Lee A. Molecular mechanism for divergent regulation of $Ca_V1.2$ Ca^{2+} channels by calmodulin and Ca^{2+}-binding protein-1. J. Biol. Chem. 2005; 280:29612–29619. [PubMed: 15980432]

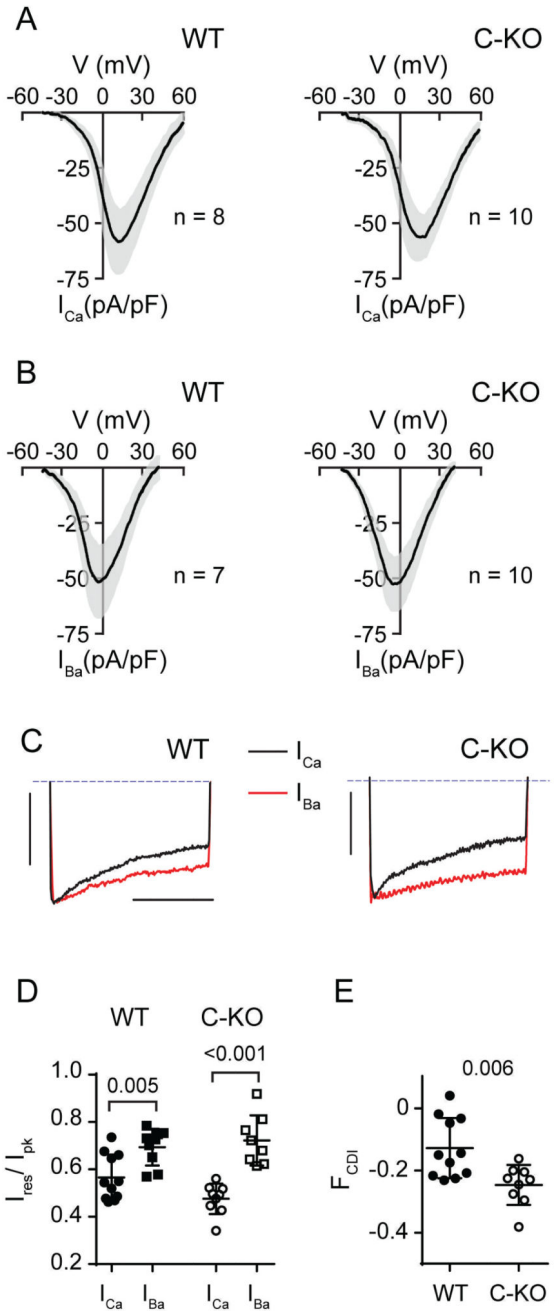

Figure 1. Voltage-dependent activation is not affected but CDI is increased in C-KO SGNs

(A–B) I–V plots for I_{Ca} (A) and I_{Ba} (B) in WT and C-KO SGNs. Voltage protocol consisted of a 320-ms ramp from −45 mV to 70 mV. Black line and grey shading represent mean and SEM, respectively. (C) Representative traces for normalized currents evoked by a 1-s step to −10 mV (for I_{Ba}) or 0 mV (for I_{Ca}) for WT and C-KO SGNs. Scale bars, 0.5 s (horizontal); 200 pA for I_{Ca} (vertical). I_{Ba} was normalized to the scale of I_{Ca}. (D) For data obtained as in *C*, inactivation was measured as current amplitude at the end of the pulse normalized to the peak current amplitude (I_{res}/I_{pk}). (E) The difference in I_{res}/I_{pk} from *D* for I_{Ca} and I_{Ba} [I_{Ca} − I_{Ba}] was plotted for WT (n = 11 cells from 9 cultures from different litters) and C-KO SGNs

(n = 9 cells from 8 cultures from different litters). Data were analyzed by unpaired t test. In *D, E*, points represent individual cells and bars represent mean ± SD; *p* values from unpaired t-tests are shown for each comparison. In *D,* $t(18) = 3.207$ for WT; $t(15) = 5.894$ for C-KO. In *E,* $t(18) = 3.143$.

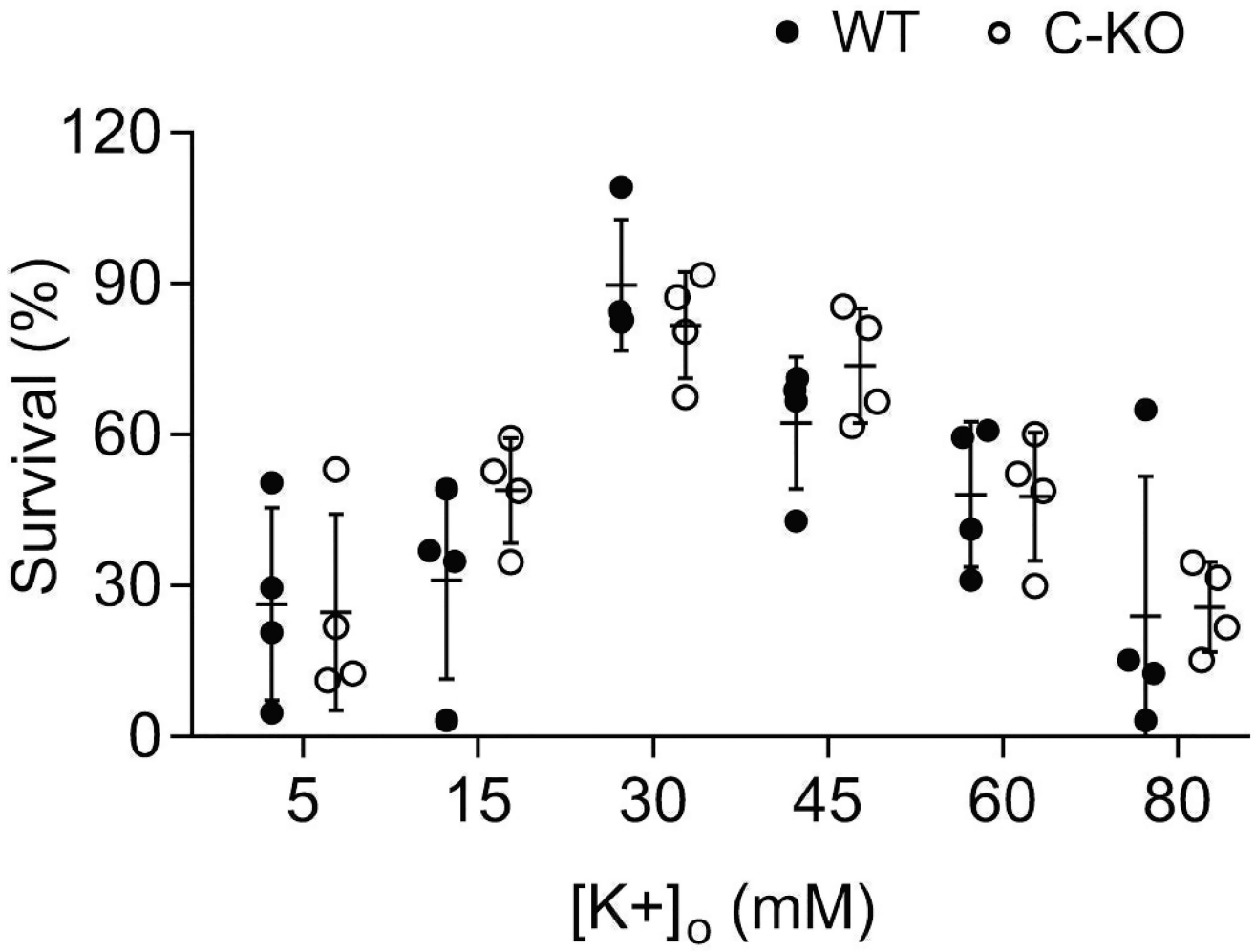

Figure 2. Activity-dependent regulation of neuron survival is not altered in C-KO SGNs

Dissociated SGNs from WT or C-KO mice were maintained in culture for 4 h prior to depolarization with different $[K^+]_o$ for 44 h prior to immunofluorescent labeling with NF200 antibodies. The control group was processed for NF200 labeling after the initial 4 h culture period. Survival (%) represents the number of SGNs at the end of depolarization period relative to the control for the indicated $[K^+]_o$. There was no significant difference in the effect of $[K^+]_o$ on SGN survival in WT and C-KO cultures ($F(1, 36) = 0.582$, $p = 0.450$, by 2-way ANOVA, n = 4 cultures each).

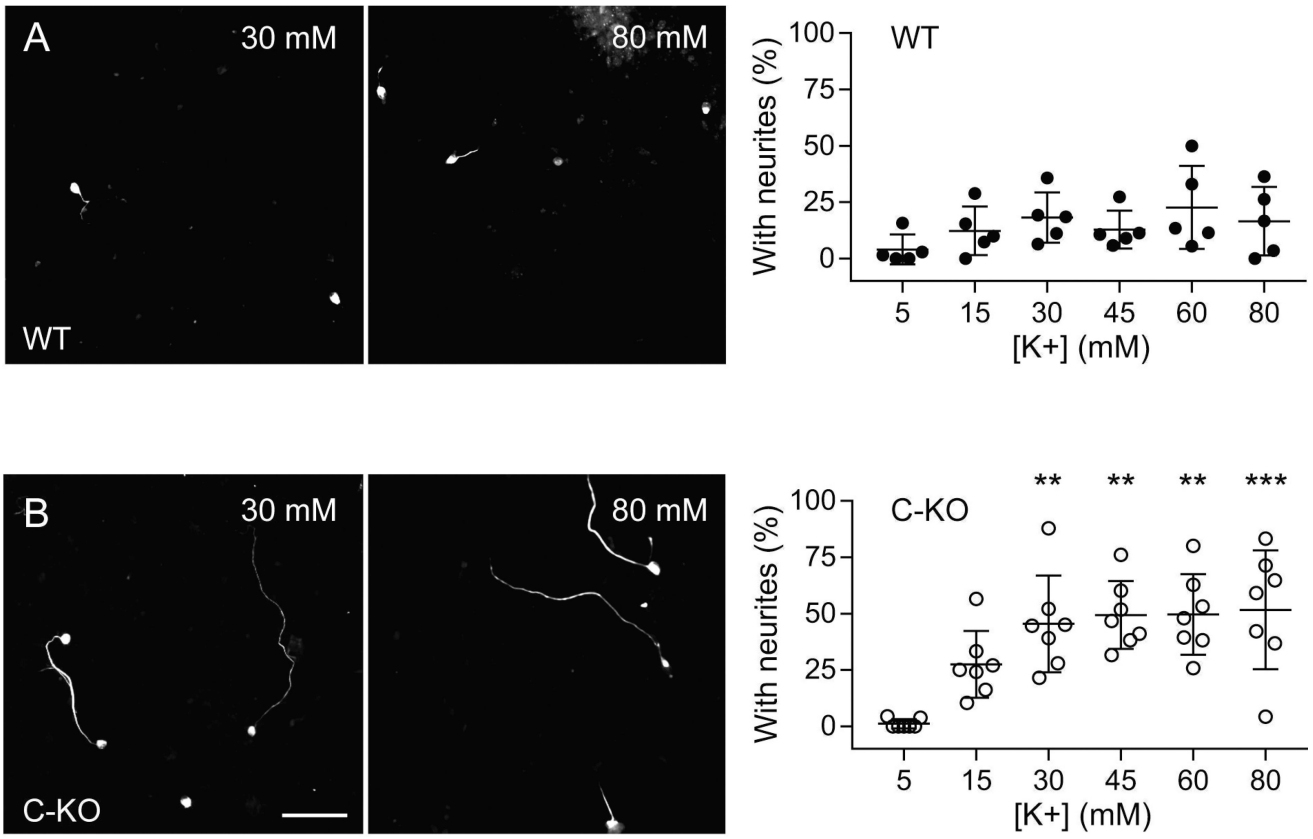

Figure 3. Activity-dependent regulation of neurite growth is altered in C-KO SGNs

Dissociated SGNs from WT or C-KO mice were maintained in culture for 4 h prior to depolarization with different $[K^+]_o$ for 44 h followed by immunofluorescent labeling with NF200 antibodies. (A,B) Representative images of WT (A) and C-KO (B) SGNs exposed to 30 mM or 80 mM $[K^+]_o$. Scale bar, 100 μm. *Right*, the percent of SGNs with neurites (relative to the total number of SGNs on the coverslip) at the end of the depolarization period is plotted for the indicated $[K^+]_o$. **, $p < 0.01$, ***, $p < 0.001$ compared to $[K^+]_o$ = 5 mM by post-hoc Dunn's multiple comparisons test. Each point represents result from different cultures (n = 5 cultures for WT, n = 7 cultures for C-KO; 3 mice were used per culture) and bars represent mean ± SD.

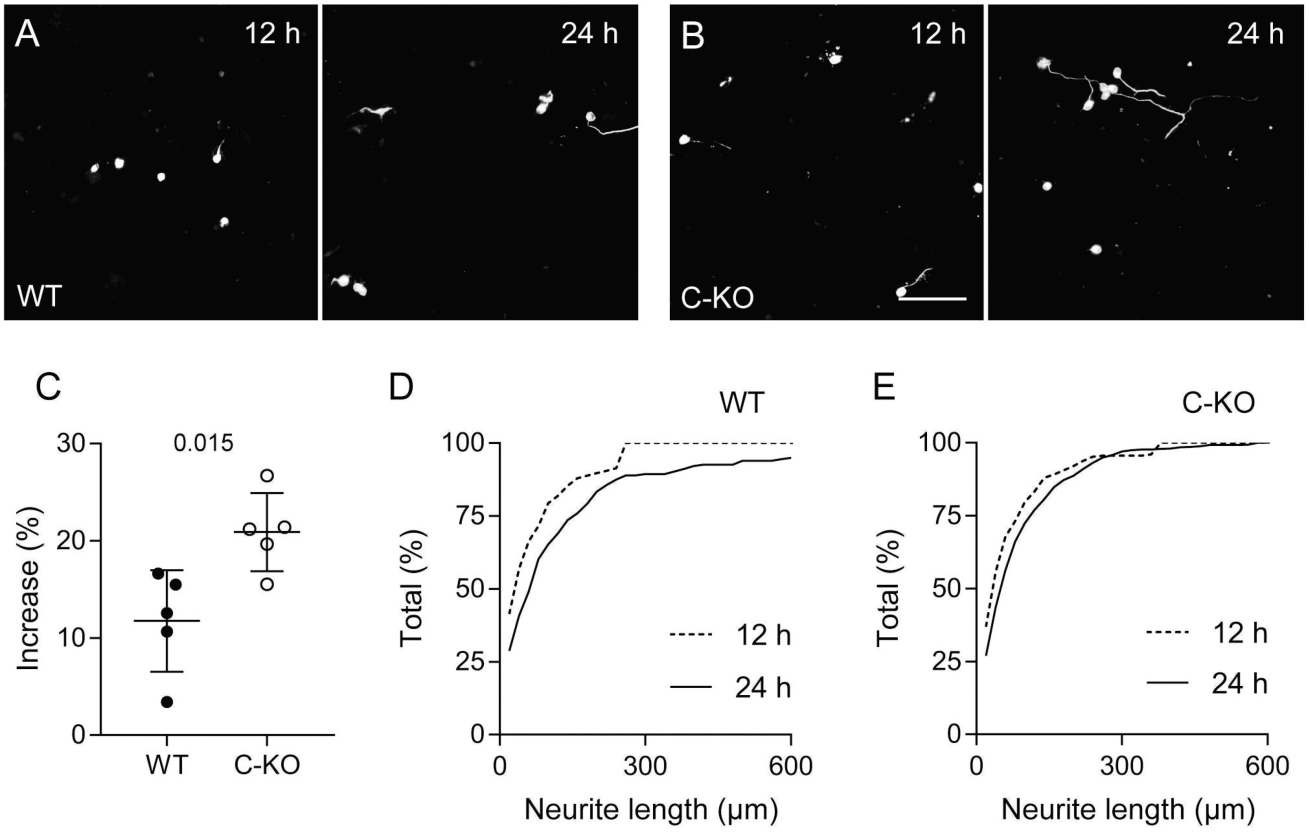

Figure 4. Neurite initiation but not rate of growth is enhanced in C-KO SGNs

SGNs were cultured for 12 h or 24 h in 30 mM $[K^+]_o$ prior to NF200 labeling. (A, B) Representative images of WT and C-KO SGNs at the indicated time points. Scale bar, 100 μm. (C) The percent increase in SGNs with neurites at 24 h relative to 12 h is shown for WT and C-KO cultures (n = 5 cultures each, two replicates for each culture; $t(8) = 3.102$, $p = 0.015$, unpaired *t* test). Each point represents result from one culture and bars represent mean ± SD. (D, E) Distribution of neurite lengths (>10 μm) for SGN cultures after 12 h and 24 h for WT (D) and C-KO (E) cultures (n = 5 each, 106 and 216 WT SGNs at 12 h and 24 h, and 265 and 667 C-KO SGNs at 12 h and 24 h were analyzed). In *D,E*, results represent measurements on all SGNs in each culture.

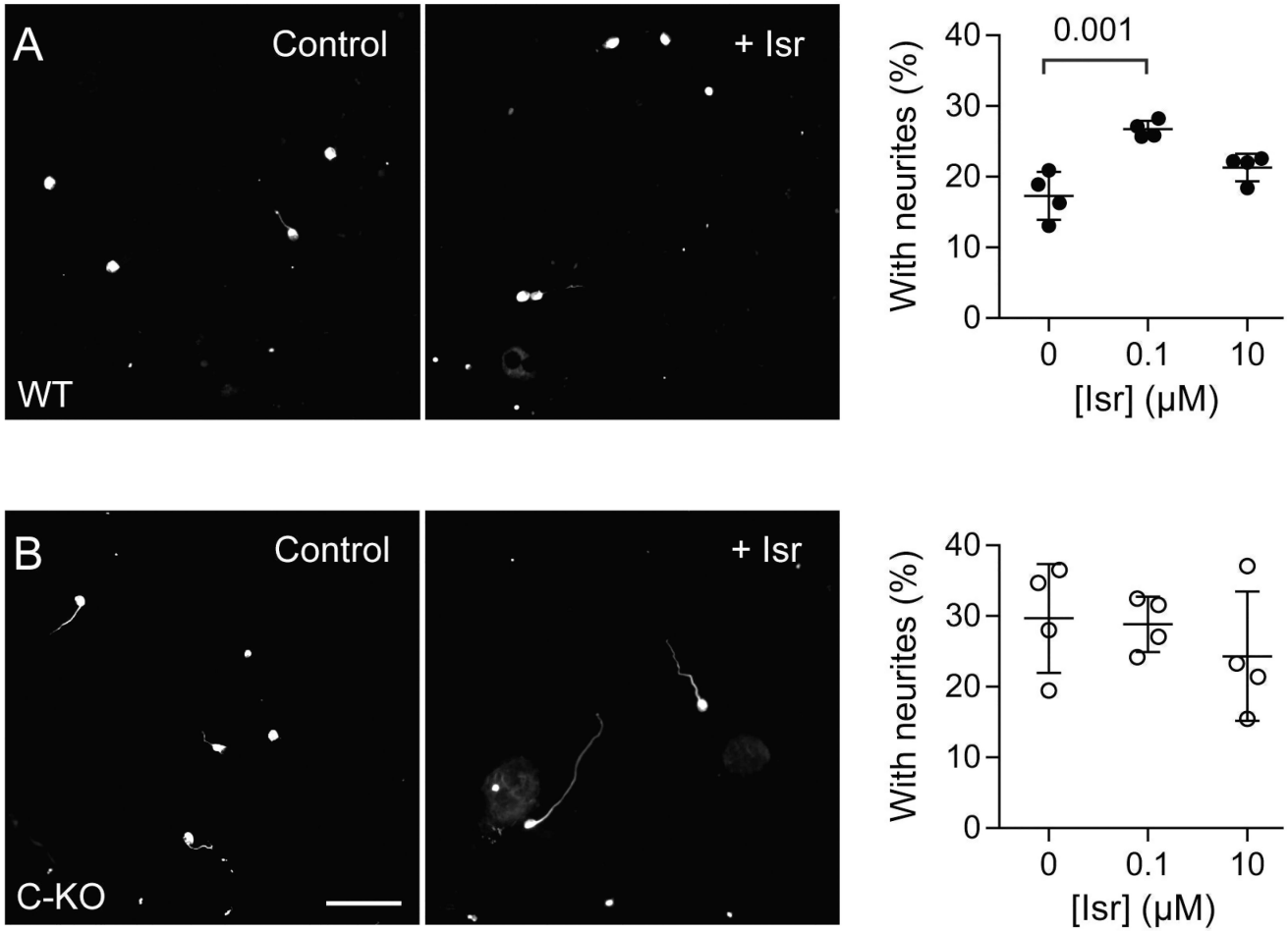

Figure 5. Isradipine nullifies difference in neurite growth in WT and C-KO SGNs

SGNs were cultured in 30 mM $[K^+]_o$ for 12 h in the presence of 0.1% DMSO or isradipine (0.1 μM or 10 μM) prior to NF200 labeling. (A,B) Representative images of WT and C-KO SGNs exposed to DMSO (control) or 0.1 μM isradipine (+ Isr). Scale bar, 100 μm. *Right*, the percentage of SGNs with neurites was measured as in Fig. 3 and shown for the indicated conditions. Isradipine had significant effects on WT SGNs ($F(2, 8) = 14.63$, $p = 0.002$ by ANOVA, n = 4 cultures/genotype), but not C-KO SGNs $F(2, 9) = 0.63$, $p = 0.56$ by ANOVA, n = 4 cultures/genotype). In *A*, *p*-value for the indicated comparison was determined by Bonferroni's post-hoc test ($t(8) = 5.374$). Each point represents result from one culture and bars represent mean ± SD.

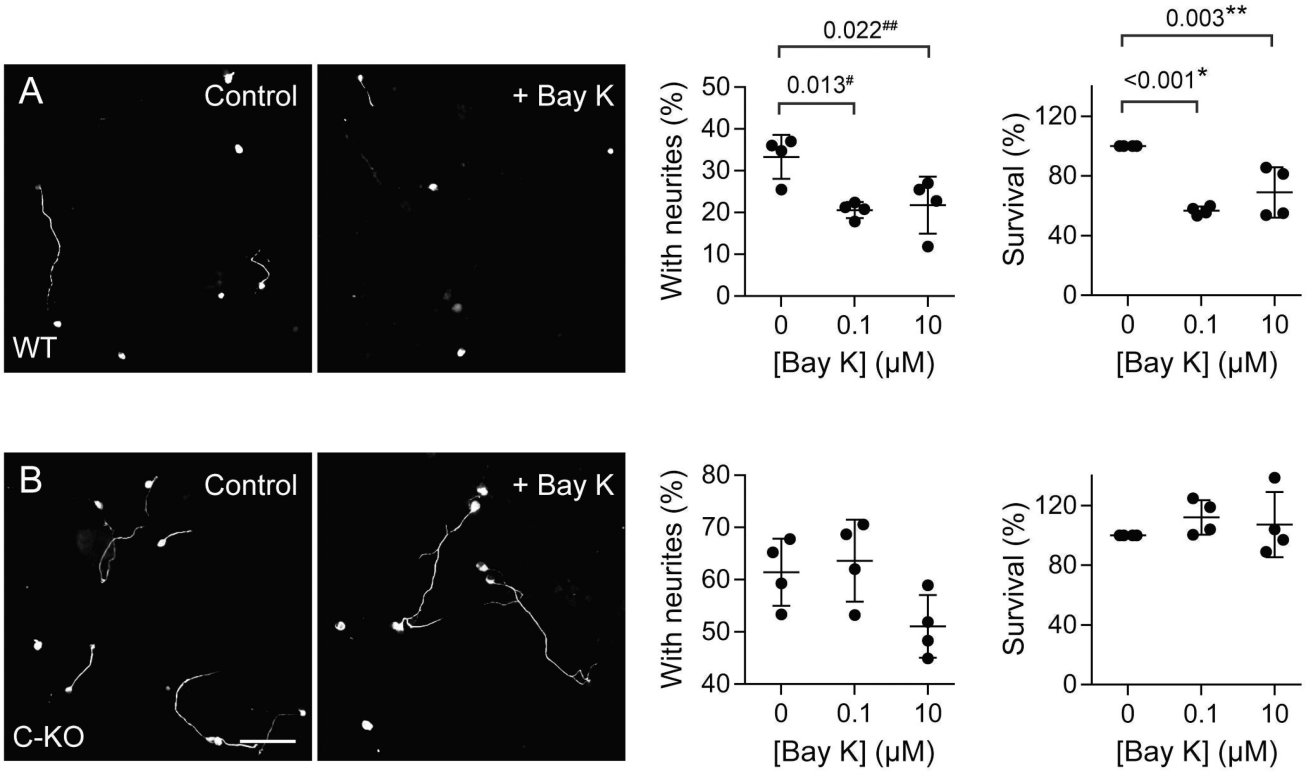

Figure 6. Bay K 8644 suppresses neurite growth and survival of WT but not C-KO SGNs

SGNs were cultured in 30 mM $[K^+]_o$ for 44 h in the presence of 0.1% DMSO or Bay K 8644 (0.1 μM or 10 μM) prior to NF200 labeling. (A,B) Representative images of WT (A) and C-KO (B) SGN cultures exposed to DMSO (control) or 0.1 μM Bay K (+ Bay K). Scale bar, 100 μm. *Right*, the percentage of SGNs with neurites was measured as in Fig. 3, and the percent survival represents the number of SGNs at the end of the depolarization period normalized to the control. Bay K had a significant effect on neurite growth ($F(2,9) = 7.57$, $p = 0.012$ by ANOVA) and survival ($F(2,9) = 20.5$, $p < 0.001$, ANOVA), but not in C-KO cultures ($F(2,9) = 3.91$, $p = 0.060$, for neurite growth and $F(2,9) = 0.72$, $p = 0.512$ for neuron survival, ANOVA). *p*-values shown for the indicated comparisons were determined by Bonferroni's test: #, $t(9) = 3.52$; ##, $t(9) = 3.19$; *, $t(9) = 6.21$; **, $t(9) = 4.45$. 4 WT and 4 C-KO cultures were analyzed. Each point represents result from one culture and bars represent mean ± SD.

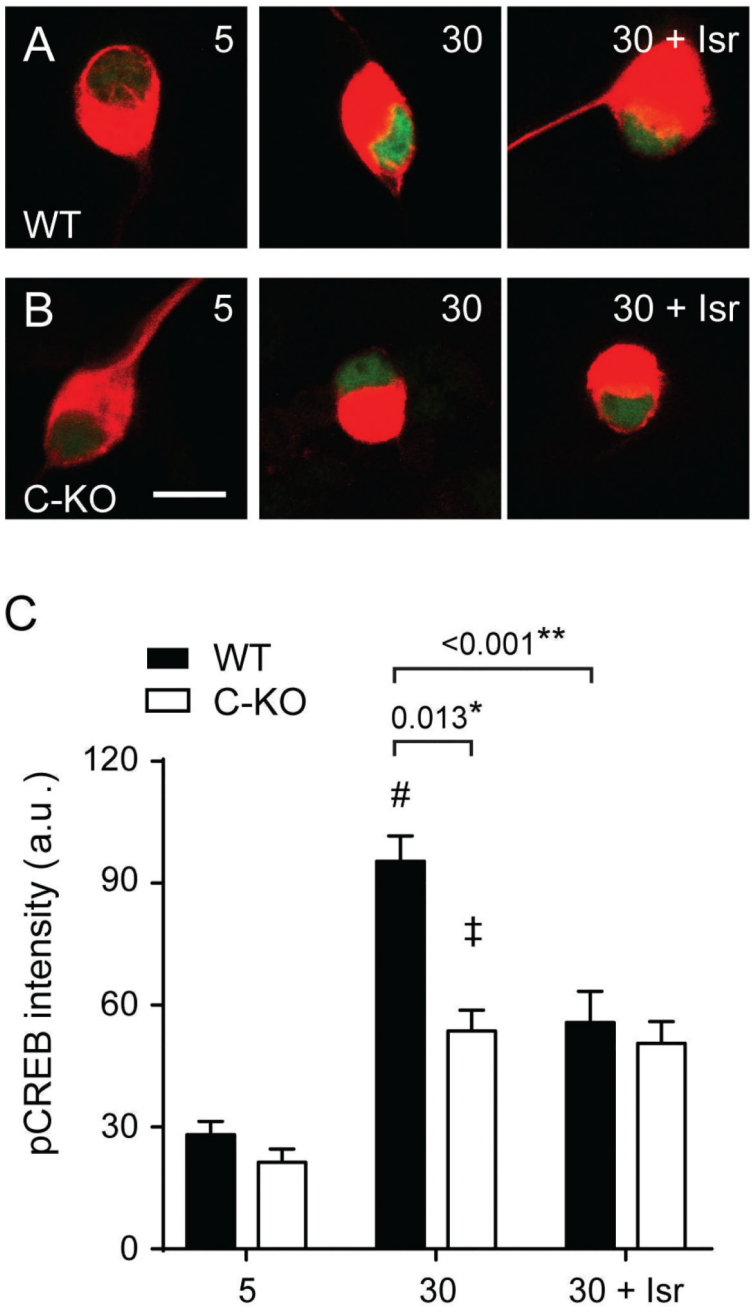

Figure 7. Ca_V1-dependent phosphorylation of CREB is abolished in C-KO SGNs

(A,B) Representative images of WT and C-KO SGNs double-labeled with antibodies against pCREB (green) and NF200 (red) following a 15-min exposure to 5 or 30 mM $[K^+]_o$ with or without isradipine (Isr, 10 μM). Scale bar, 10 μm. (C) Quantification of pCREB intensity in arbitrary units (a.u.). Results represent analyses of ~56 SGNs in 3 independent cultures. Each culture was prepared from 8 pups with 2 technical replicates per condition. 8–10 neurons were randomly selected from each replicate. Data are plotted as mean ± SEM. By Kruskal-Wallis and post-hoc Dunn's test: #, compared to WT 5 mM, $p_{adj} < 0.001$ with mean rank difference of 171.9; ǂ, compared to C-KO 5 mM, $p_{adj} < 0.001$ with mean rank

difference of 144.4; p-values are shown for the indicated comparisons. *, mean rank difference = 76.28; **, mean rank difference =104.9.

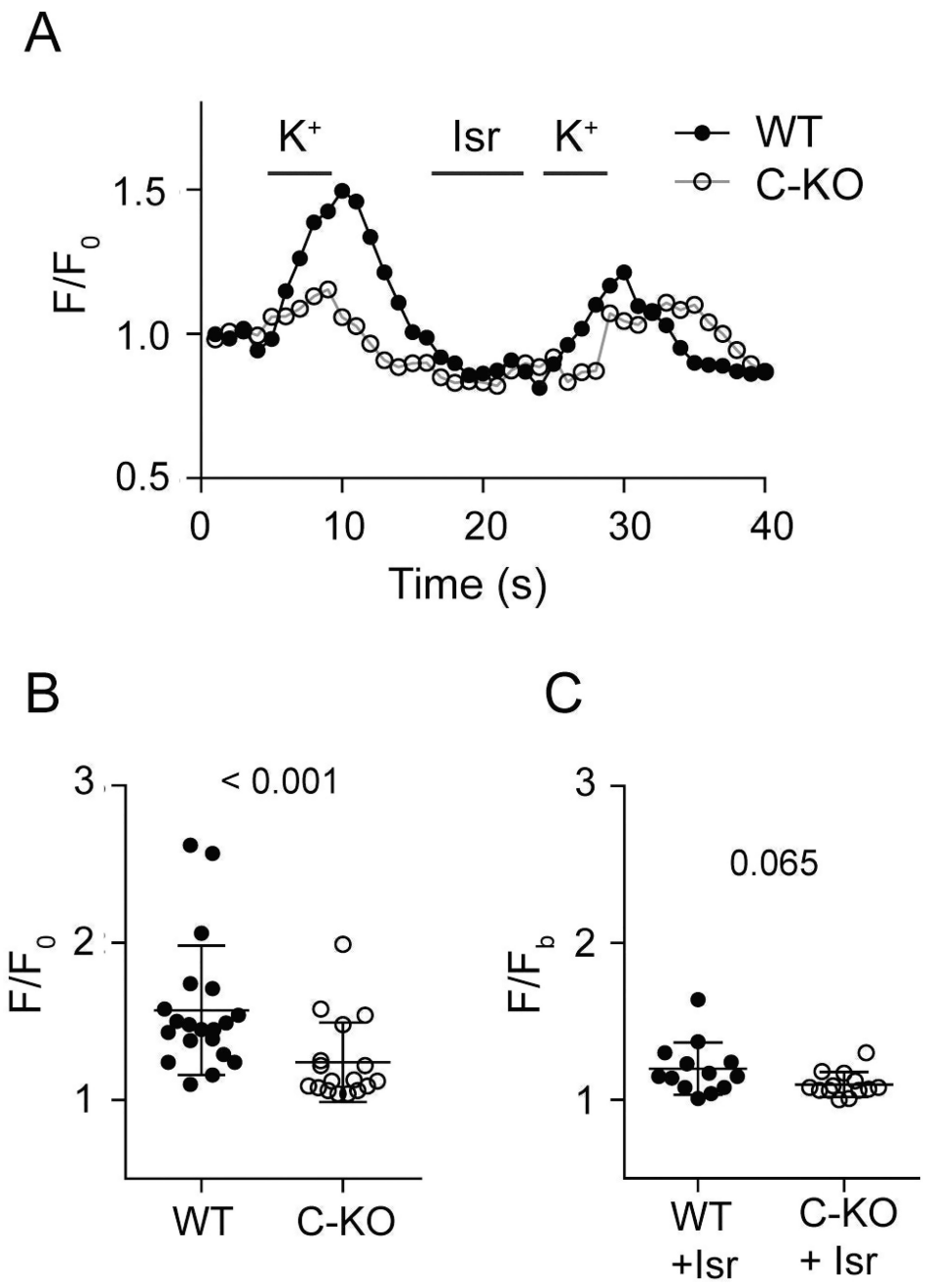

Figure 8. Ca_V1-mediated Ca^{2+} signals are reduced in C-KO SGNs

(A) Representative changes in GCaMP3 fluorescence (F/F_0) in SGNs from WT or C-KO mice evoked by 80 mM $[K^+]_o$ before and after application of isradipine. (B,C) Quantification of GCaMP3 fluorescent intensity changes in data obtained in *A*. *p*-values determined by Mann-Whitney test are indicated. $U = 68.5$ in *B*, $U = 48.5$ in *C*. Each point represents one region of interest and bars represent mean ± SD. F, maximum intensity; F_0, intensity at time 0; F_b, baseline intensity. Data were collected from 4 WT and 4 C-KO cultures prepared from different litters. Each culture was prepared from 2–3 pups. For each experiment, 1–3 regions of interest were analyzed.

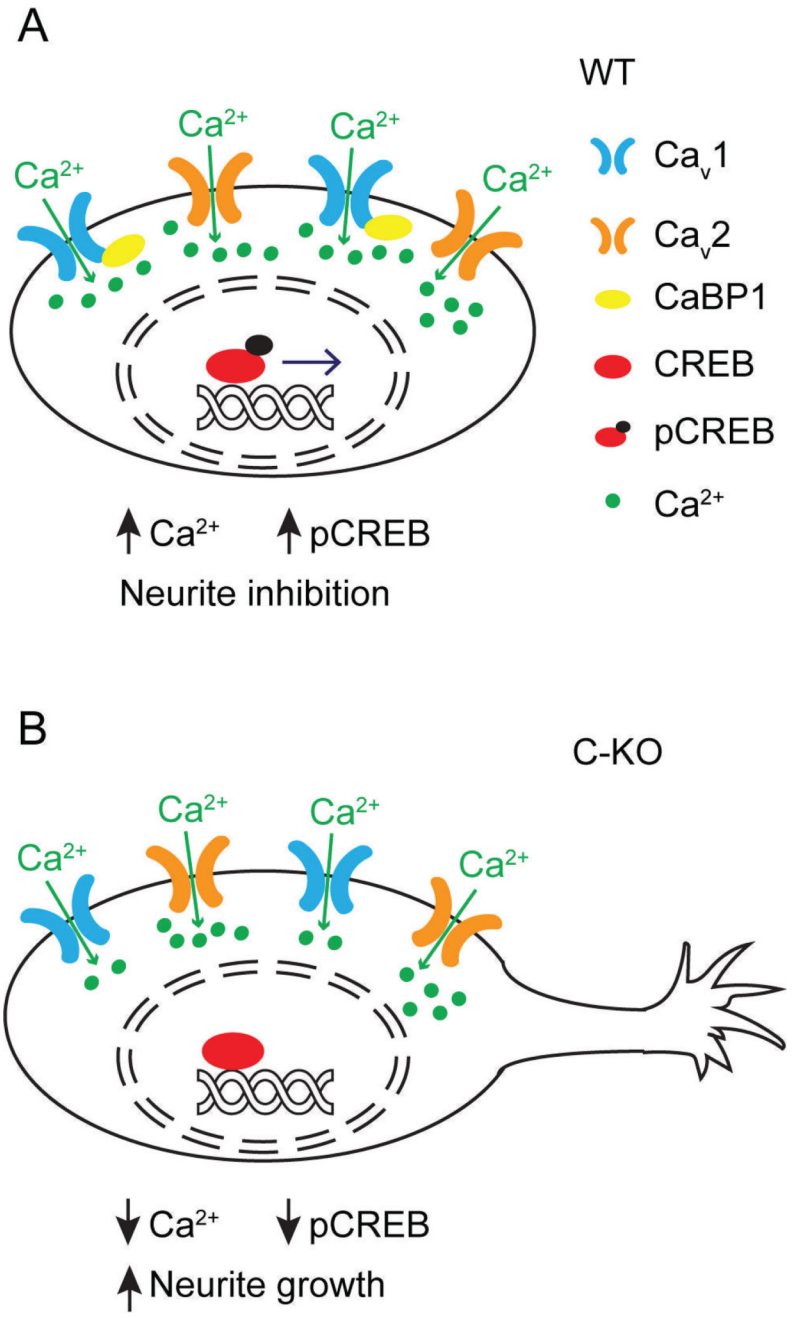

Figure 9. Ca_v1 signaling pathways that are altered in C-KO SGNs

(A) In WT SGNs, CaBP1 reduces CDI of Ca_v1 channels leading to increased Ca_v1-mediated signaling to pCREB and repression of neurite growth. (B) In C-KO SGNs, Ca_v1 channels undergo increased CDI and less coupling to pCREB and derepression of neurite growth.

Table 1

Parameters from Boltzmann fits of I–V data

		WT (n = 10)	C-KO (n = 10)	*t* – and *p* – values
I_{Ca}	V_h (mV)	1.18 ± 1.12	1.05 ± 1.39	$t(20) = 0.072$, $p = 0.944$
	k (mV)	6.13 ± 0.36	6.55 ± 0.53	$t(20) = 0.656$, $p = 0.519$
	$I(pA/pF)_{max}$	−62.69 ± 8.93	−56.35 ± 6.81	$t(20) = 0.574$, $p = 0.573$
I_{Ba}	V_h (mV)	−15.56 ± 1.50	−17.44 ± 1.12	$t(18) = 1.029$, $p = 0.317$
	k (mV)	8.12 ± 0.48	8.97 ± 0.51	$t(18) = 1.197$, $p = 0.247$
	$I(pA/pF)_{max}$	−54.07 ± 7.36	−52.32 ± 5.24	$t(20) = 0.199$, $p = 0.845$

Data represent mean ± SEM; *t* – and *p* – values determined by unpaired *t* – test.

Table 2

Effect of isradipine on survival WT and C-KO SGNs.

[Isr] (μM)	WT (% survival)	C-KO (% survival)
0.1	90.94 ± 10.68	88.57 ± 10.46
10	62.07 ± 2.70***	56.63 ± 2.43***

SGNs were cultured in 30 mM $[K^+]_O$ for 12 h in the presence of 0.1% DMSO (control) or isradipine (0.1 μM or 10 μM) prior to NF200 labeling. Percent survival represents the number of SGNs at the relative to the vehicle control at the end of the depolarization period. By 2-way ANOVA, isradipine had a significant effect ($F(2, 18) = 22.68$, $p < 0.001$; n = 4 cultures/genotype), but there was no difference between genotypes ($F(1, 18) = 0.26$, $p = 0.617$).

*** % survival was significantly reduced compared to control, $p < 0.001$ ($t(18) = 4.27$ for WT;

** $t(18) = 4.89$ for C-KO), Bonferroni's post-hoc test.